Quantifying the Impact of Coincidental Versus Preferential Seam Weld Corrosion

Michael Turnquist[1], Yanping Li[2], Yohann Miglis[3]
[1]Quest Integrity, [2]Enbridge, [3]Kinder Morgan

Pipeline Pigging and Integrity Management Conference

February 12-16, 2024

Organized by
Clarion Technical Conferences

https://doi.org/10.52202/072781-0005

https://doi.org/10.52202/072781-0005

Abstract

A critical factor in determining the remaining strength of a corrosion feature intersecting a longitudinal seam weld (LSW) is whether the corrosion is preferential to the weld (often referred to as selective seam weld corrosion or SSWC) or coincident with the weld yet no preferential attack of the bondline is occurring. SSWC is a form of corrosion that most often occurs in the bondline of electric resistance welded (ERW) and electric flash welded (EFW) pipe and typically has the appearance of a V-shaped groove. Past research supports that if no preferential attack of the LSW bondline is occurring and the weld has adequate ductility, the presence of the LSW does not reduce the remaining strength of the feature when compared to features not intersecting the LSW, and that industry accepted corrosion assessment models are suitable.

This paper provides an overview of additional full-scale destructive testing and detailed engineering analysis that further supports the observation that under most realistic conditions associated with the operation of liquid pipelines, the presence of an LSW does not negatively impact the remaining strength of the corrosion feature. Potential exceptions to this behavior relate to the ductility of the weld, constraint effects and morphology from the feature geometry, operating stress of the pipe, and whether or not preferential attack of the LSW bondline is occurring.

The work presented in this paper is part of the Pipeline Research Council International (PRCI) project EC-02-13 "Response to Corrosion Interacting with the Longitudinal Seam in Liquid Pipelines." The objectives of this project are to clarify which analysis methodologies are appropriate to assess corrosion coincident with a pipeline LSW and to support the development of recommended guidelines for effective management of these types of features. This work is being executed in parallel with sibling projects EC-02-12 "Evaluation of Selective Seam Weld Corrosion Susceptibility," NDE-4-13 "Selective Seam Weld Corrosion Detection with In-line Inspection Technologies," IM-3-03 "Comprehensive Review and Assessment Guidelines for SSWC," IM-1-08 "Pragmatic Application of MegaRule RIN 1 - 192.712 Toughness Values," and NDE-2-15 "SSWC Identification, Sizing, and Measuring Grooving Ratio In the Ditch."

Introduction

The primary objectives of project EC-02-13 "Response to Corrosion Interacting with the Longitudinal Seam in Liquid Pipelines" are to clarify which analysis methodologies are appropriate to assess corrosion coincident with a pipeline LSW and to support the development of recommended guidelines for effective management of these types of features.

The overall project scope includes execution of destructive testing of corrosion features intersecting a longitudinal seam weld, material property testing of longitudinal seam welds produced by multiple

https://doi.org/10.52202/072781-0005

manufacturing methods, detailed engineering analysis, and a literature review of all past relevant research. This paper covers the following topics:

- A summary of relevant past research on the topic of quantifying the remaining strength of corrosion features intersecting an LSW.
- An overview of the destructive testing executed as part of this project, including full-scale testing and material property testing.
- A description of the detailed engineering analysis utilized to further supplement the observations from the full-scale testing.

The final deliverable for this project is guidelines and criteria to effectively manage corrosion intersecting an LSW. At the time of this writing, these guidelines have not yet been fully developed. However, this document will provide a preview of these guidelines based on the observations and learnings from this project to date. In addition to the learnings from the project tasks discussed herein, the final guidelines will consider the susceptibility of the affected pipeline to SSWC and the capability of different inspection technologies (i.e., ILI and in-ditch) to effectively identify and characterize potential SSWC. These guidelines will serve as the basis for recommendations to revise the language of CFR 195.452 and API RP 1176.

Summary of Relevant Past Research

This section contains an overview of past research supporting that if no preferential attack of the LSW bondline is occurring and the weld has adequate ductility, the presence of the LSW does not reduce the remaining strength of the feature when compared to features not intersecting the LSW, and that industry accepted corrosion assessment models are suitable.

Battelle Research Team (2004 to 2006)

From 2004 to 2006, a Battelle research team published multiple documents on the subject of corrosion at LSWs and girth welds [1] [2] [3], one of which was prepared for the Pipeline and Hazardous Materials Safety Administration (PHMSA). The key objectives were to develop guidelines allowing the safe use of existing remaining strength and engineering critical prediction methods to assess corrosion occurring at an LSW or a girth weld, and to develop data that validate these guidelines and identify circumstances in which the guidelines would be inappropriate.

The Battelle research also evaluated full-scale and laboratory testing, as well as a publicly available database of documented in-service failures. Part of this research considered a selection of three field failures involving girth weld and LSW corrosion complemented by selected laboratory test data and related analysis. The observed trends from this review supported the above discussion that constraint is a key contributor to the remaining strength of a corrosion feature at a weld. The presence of high

https://doi.org/10.52202/072781-0005

constraint was observed to nucleate cracking in lower-toughness steels. In contrast, in the absence of high constraint, evidence of plastic collapse behavior was observed.

The Battelle research identified the following key factors to consider when determining appropriateness of a traditional metal loss assessment model for corrosion at a weld:

- The seam is free of crack-like flaws at the location of the corrosion.
- The corrosion geometry does not result in high shape-induced constraint.
- The mechanical properties of the seam are equivalent to, or more favorable than, those of the pipe body.
- The fracture properties of the seam are adequate to ensure failure is controlled by plastic collapse.
- The service and environmental conditions do not introduce the potential for an environmental cracking concern, such as stress corrosion cracking (SCC).
- The local loading conditions are consistent with the design conditions such that high constraint is not induced within the corrosion feature.

PHMSA Subtask 1.4 (2012) and Subtask 2.2 (2013)

From 2012 to 2013, PHMSA sponsored research to better understand the behavior of ERW and EFW seams. Subtask 1.4 of this research consisted of the review of a database of 576 seam weld related failures [4] [5]. The causes of failure contained in this database included SSWC and initial manufacturing defects (i.e., cold welds, hook cracks, and other anomalies related to initial manufacturing). Of significant note, no failures contained in the database were documented as being caused by a typical blunt metal loss feature that was coincident, but not preferential to, the LSW.

As a follow-up to Subtask 1.4, Subtask 2.2 of this research presented the results of three full-scale burst tests conducted on samples containing manufacturing anomalies in early vintage ERW seams [6]. Charpy V-notch (CVN) impact testing of the seam welds determined that the ductile-to-brittle transition temperatures (DBTTs) of each sample exceeded 139°F (59°C), although it should be noted that these impact test results do not necessarily indicate low fracture toughness at the burst test temperatures due to the uncertainty related to correlating CVN impact energy with fracture toughness. All three tests were observed to burst at pressures approximately equal to or greater than the predicted burst pressure using the modified Ln-Secant equation [7] when assuming an upper-shelf CVN impact energy associated with ductile material behavior.

Although the modified Ln-Secant equation is typically used to estimate the remaining strength of crack-like features, when an upper-shelf CVN impact energy associated with ductile material behavior is assumed, the results will be similar to the application of a traditional effective area-based metal loss assessment model. This implies that, even though the samples that were subjected to burst testing likely exhibited low toughness in the seam, their burst pressures were similar to what would have been predicted by applying a traditional metal loss assessment model.

https://doi.org/10.52202/072781-0005

These results provide direct examples of instances when the remaining strength of blunt corrosion features coincident with, but not preferential to, an LSW could be reliably evaluated using a traditional metal loss assessment model. While Subtask 1.4 provides cautionary statements about the presence of SSWC and its effect on remaining strength, this research provided no evidence that corrosion merely coincident to the LSW could not be reliably analysed using a traditional metal loss assessment model.

Additional Burst Test Data

Similar research to the above has been conducted over the past 50+ years, the earliest of which is documented in a paper presented at the American Gas Association's 4th Symposium on Line Pipe Research in 1969 [8]. This paper details the execution of multiple burst tests of machined notches and simulated corrosion features present in pipe samples with high DBTTs, several of which features were coincident with ERW and EFW seams. Metallurgical analysis of the fracture surfaces indicated ductile fracture initiation (albeit brittle propagation). Similar behavior was also observed during testing conducted as part of a 2007 PRCI report (PR276-04502) [9].

Additional relevant burst test data were presented at the 2004 International Pipeline Conference in Calgary, Alberta [10]. The paper described burst testing of notches and simulated corrosion features located on downhole well casing. The material specifications for these samples included API 5CT grades J-55 and K-55, as well as API 5L Grade A. CVN impact testing indicated that the samples had high DBTTs, although it should be noted that these impact test results do not necessarily indicate low fracture toughness at the burst test temperatures due to the uncertainty related to correlating CVN impact energy with fracture toughness. A total of seven burst tests were executed. For all tests, the samples were either observed to fail at a pressure significantly greater than the failure pressure that a traditional effective area-based metal loss model would predict, or no failure was observed up to pressures of 100% of the specified minimum yield strength (SMYS) or greater.

Additional Studies

A paper presented at the 2022 Pipeline Pigging and Integrity Management conference in [11] summarized the above research and presented the results of fracture mechanics analyses that were conducted to better understand the potential behavior of corrosion features coincident with a seam weld. Burst pressure calculations were executed for crack-like features assumed to be located in pipes with multiple dimensions and grades. Calculations were executed using the MAT-8 fracture model and the theoretical basis for the CorLAS fracture model, both of which have been accepted by the industry as applicable to accurately model both ductile and brittle material behavior.

If the tip radius of a notch-like feature is large enough, the feature is expected to fail from plastic collapse. Equations 5.11, 5.16, and 5.17 in API 579-1/ASME FFS-1 [12] (API 579) Part 5 use the tip

https://doi.org/10.52202/072781-0005

radius to determine whether a metal loss feature should be treated as a local thinned area (LTA), groove, or crack. If the tip radius is large enough, the feature can be treated as an LTA that is expected to fail from plastic collapse. The concentration of stress increases as the tip radius decreases, and the relevant failure mode shifts toward brittle fracture. The technical basis for these criteria is documented in a study executed by Quest Integrity and the American Society of Mechanical Engineers [13]. One key concept from this study is that, as flaw tip radius decreases and the flaw behaves more like a crack, the effective burst pressure of the feature will decrease, as demonstrated in **Figure 1**. Based on this concept, the application of a fracture mechanics model such as MAT-8 or CorLAS will provide a lower-bound prediction of remaining strength when applied to a metal loss feature, groove-like feature, or notch-like feature.

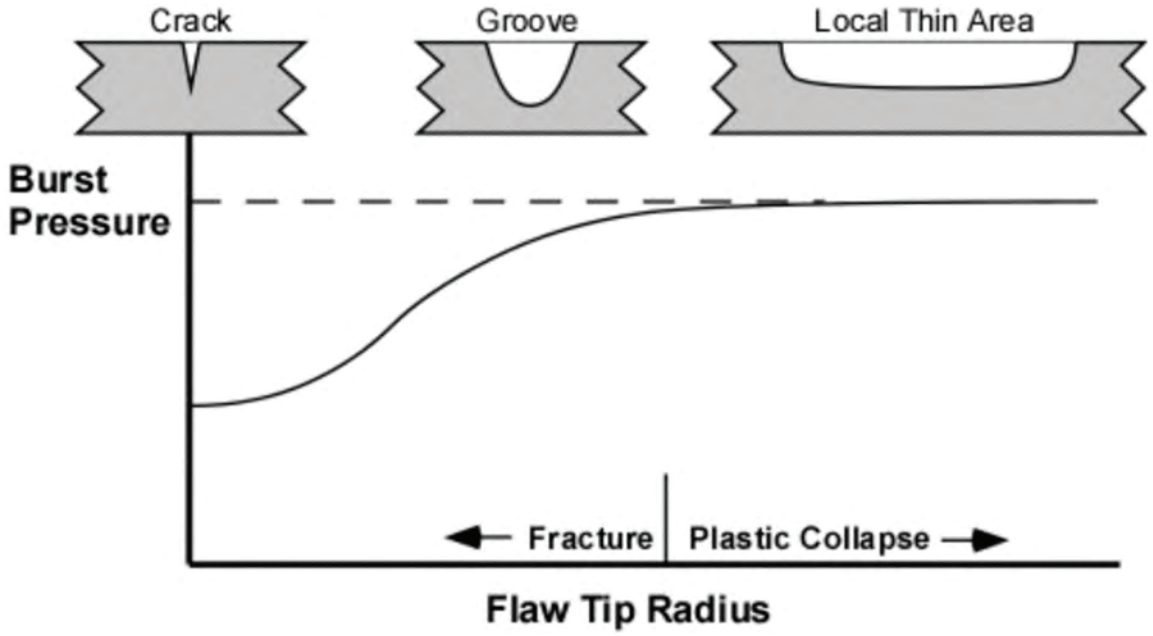

Figure 1. Effect of notch acuity on burst pressure for a given material, flaw length, and flaw depth.

Critical depths were calculated for flaws assumed to be of infinite length, representing a worst-case scenario. The results of the fracture mechanics analyses indicated that, when operating at a stress level of 50% SMYS or less, an infinitely long flaw would be predicted to be stable for a depth of up to 30% of the corresponding wall thickness. Applying a fracture mechanics model such as MAT-8 or CorLAS provides a lower-bound prediction of remaining strength when applied to a metal loss feature, thus indicating that plastic collapse behavior would be expected for any metal loss flaw with a depth ≤ 30% of the corresponding wall thickness, given the operating stress is 50% SMYS or less.

Likewise, the results of the fracture mechanics analyses indicated that when operating at a stress level exceeding 50% SMYS, an infinitely long flaw would be predicted to be stable for a depth of up to 20% of the corresponding wall thickness. This indicates if the operating stress exceeds 50% SMYS,

https://doi.org/10.52202/072781-0005

plastic collapse behavior would be expected for any metal loss flaw with a depth ≤ 20% of the corresponding wall thickness.

Combining the fracture mechanics analysis results with the past research described herein produced the following recommended guidelines to assess metal loss features at an LSW. These guidelines were developed to identify circumstances under which it may not be appropriate to utilize a traditional metal loss model to assess remaining strength of a corrosion feature located at a longitudinal seam. These instances include:

- Evidence of the corrosion being preferential to the seam (i.e., SSWC)
- Evidence of existing linear indications in the seam
- The seam type is direct current ERW, low-frequency ERW, or EFW, unless it can be confirmed that the CVN impact energy exceeds 4 ft-lbs (or the fracture toughness exceeds 34.85 ksi√inch)
- For operating stresses ≤ 50% SMYS, the metal loss depth is > 30% of the corresponding wall thickness
- For operating stresses > 50% SMYS, the metal loss depth is > 20% of the corresponding wall thickness

These guidelines were described by the author as being conservative. Furthermore, the author recommended additional burst testing and finite element analysis (FEA) of corrosion features coincident with seam welds to further refine these guidelines and reduce excess associated conservatism.

Destructive Testing

To quantify the remaining strength of metal loss features coincident with an LSW, yet not preferential to the LSW, corrosion anomalies were installed along the LSW using electrical discharge machining (EDM). Four different-sized corrosion features and four types of LSW manufacturing processes were investigated, resulting in 16 total samples. These features would be classified as either axial slotting or axial grooving based on API 1163 Figure 3 [14]. Furthermore, API 579 equations 5.11, 5.16, and 5.17 would recommend these features be assessed as a traditional LTA as opposed to a groove or crack. **Table 1** summarizes the testing matrix.

https://doi.org/10.52202/072781-0005

Table 1. Samples Considered for Destructive Testing

Sample No.	Seam Type	Outside Diameter (OD), inch	Wall Thickness (WT), inch	Feature Depth, %WT	Feature Width	Feature Length, inch
LF1	Low frequency (LF) ERW	10.75	0.219	30 %	1 x WT	3.0
LF2				50 %	1 x WT	3.0
LF3				30 %	3 x WT	3.0
LF4				50 %	3 x WT	3.0
HF1	High frequency (HF) ERW	12.75	0.250	30 %	1 x WT	3.0
HF2				50 %	1 x WT	3.0
HF3				30 %	3 x WT	3.0
HF4				50 %	3 x WT	3.0
AO1	EFW (AO Smith)	12.75	0.250	30 %	1 x WT	3.0
AO2				50 %	1 x WT	3.0
AO3				30 %	3 x WT	3.0
AO4				50 %	3 x WT	3.0
DSAW1	Double submerged Arc Welded (DSAW)	18.0	0.312	30 %	1 x WT	3.0
DSAW2				50 %	1 x WT	3.0
DSAW3				30 %	3 x WT	3.0
DSAW4				50 %	3 x WT	3.0

Following installation of the corrosion features, additional corrosion was intentionally generated on its surface to achieve a more realistic corrosion profile, including the introduction of a local pitted surface. The external surfaces of each corrosion feature were scanned using a Creaform laser scan tool prior to execution of testing to support the additional engineering analysis described in a later section of this paper.

Material Property Testing

A sample of pipe representing each of the four seam types considered was subjected to tensile testing, CVN impact testing, and J-R testing per ASTM E1820 [15] to directly measure fracture toughness. The material property testing results for each seam type are summarized in Table 2 through Table 5.

https://doi.org/10.52202/072781-0005

Table 2. Material Property Testing Results, LF ERW

Tensile Testing		
Sample Orientation	**Yield Strength, psi**	**Ultimate Tensile Strength, psi**
Transverse (Body)	63,500	90,400
Transverse (Weld)	-	94,800

CVN Impact Testing						
Test Temperature (°F)	**Specimen Size**	**Location**	**% Shear**	**Impact Energy, ft-lbs**	**Equivalent K_{mat}[1] (psi√inch)**	
					5% Lower Bound	**50% Median**
50	0.33	Body	70	8	55,101	89,133
			90	9	62,878	104,045
			100	9.5	103,730	122,473
50	0.33	Bondline	20	3	47,665	74,859
			10	3	54,590	88,153
			20	2	35,307	51,184
50	0.33	HAZ	80	8	55,276	89,469
			60	6.5	50,821	80,929
			60	7.5	54,390	87,771

J-R Testing	
Location	**K_J (psi√inch)**
Body	83,511
Bondline (1)	88,860
Bondline (2)	Invalid[2]
Bondline (3)	47,975
Bondline (4)	51,313

[1] For observed % shear values indicative of upper shelf behavior (i.e., 100%), the equivalent K_{mat} value was computed using the Wallin upper shelf correlation. For observed % shear values indicative of the transition region, the equivalent K_{mat} value was computed using the Master Curve method in API 579 Annex 9F.

[2] Complications existed in obtaining valid J-R test results due to the specimen size and the load range, causing difficulties with obtaining consistent crack growth within each testing step.

https://doi.org/10.52202/072781-0005

Table 3. Material Property Testing Results, HF ERW

Tensile Testing		
Sample Orientation	**Yield Strength, psi**	**Ultimate Tensile Strength, psi**
Transverse (Body)	65,500	75,600
Transverse (Weld)	-	72,800

CVN Impact Testing						
Test Temperature (°F)	**Specimen Size**	**Location**	**% Shear**	**Impact Energy, ft-lbs**	**Equivalent K_{mat}[1] (psi√inch)**	
					5% Lower Bound	**50% Median**
50	0.33	Body	100	46	284,660	336,094
			100	48	292,520	345,374
			100	50	300,263	354,517
50	0.33	Bondline	100	42	228,760	317,085
			100	42	228,760	317,085
			100	40	221,727	307,337
50	0.33	HAZ	100	52	262,266	363,528
			100	50	255,765	354,517
			100	45	239,087	331,400

J-R Testing	
Location	**K_J (psi√inch)**
Body	256,342
Bondline (1)	96,342
Bondline (2)	Invalid[2]
Bondline (3)	64,502
Bondline (4)	Invalid[2]

[1] For observed % shear values indicative of upper shelf behavior (i.e., 100%), the equivalent K_{mat} value was computed using the Wallin upper shelf correlation. For observed % shear values indicative of the transition region, the equivalent K_{mat} value was computed using the Master Curve method in API 579 Annex 9F.

[2] Complications existed in obtaining valid J-R test results due to the specimen size and the load range, causing difficulties with obtaining consistent crack growth within each testing step.

https://doi.org/10.52202/072781-0005

Table 4. Material Property Testing Results, EFW (AO Smith)

Tensile Testing		
Sample Orientation	**Yield Strength, psi**	**Ultimate Tensile Strength, psi**
Transverse (Body)	53,300	77,500
Transverse (Weld)	-	79,800

CVN Impact Testing						
Test Temperature (°F)	**Specimen Size**	**Location**	**% Shear**	**Impact Energy, ft-lbs**	**Equivalent K_{mat}[1] (psi√inch)**	
					5% Lower Bound	**50% Median**
50	0.5	Body	30	5	52,567	84,276
			30	4	41,654	63,352
			30	3.5	44,292	68,410
50	0.33	Bondline	20	2	37,579	55,539
			20	1.5	38,165	56,663
			10	1.5	42,216	64,430
50	0.33	HAZ	40	4.5	51,031	81,331
			40	4	47,428	74,422
			40	4.5	51,031	81,331

J-R Testing	
Location	**K_J (psi√inch)**
Body (1)	94,819
Body (2)	96,723
Bondline (1)	107,725
Bondline (2)	102,594
Bondline (3)	94,819

[1] For observed % shear values indicative of upper shelf behavior (i.e., 100%), the equivalent K_{mat} value was computed using the Wallin upper shelf correlation. For observed % shear values indicative of the transition region, the equivalent K_{mat} value was computed using the Master Curve method in API 579 Annex 9F.

https://doi.org/10.52202/072781-0005

Table 5. Material Property Testing Results, DSAW

Tensile Testing		
Sample Orientation	**Yield Strength, psi**	**Ultimate Tensile Strength, psi**
Transverse (Body)	63,600	78,400
Transverse (Weld)	-	80,400

CVN Impact Testing						
Test Temperature (°F)	**Specimen Size**	**Location**	**% Shear**	**Impact Energy, ft-lbs**	**Equivalent K_{mat}[1] (psi√inch)**	
					5% Lower Bound	**50% Median**
50	0.5	Body	60	9.5	57,819	94,344
			60	8	51,217	81,688
			60	10	59,512	97,591
50	0.5	Bondline	70	19	79,132	135,210
			70	20	80,486	137,805
			70	19.5	79,821	136,530
50	0.5	HAZ	80	18	82,041	140,786
			80	17.5	81,139	139,056
			80	17	80,196	137,248

J-R Testing	
Location	**K_J (psi√inch)**
Body (1)	80,049
Bondline (1)	142,461
Bondline (2)	149,700
Bondline (3)	147,326

[1] For observed % shear values indicative of upper shelf behavior (i.e., 100%), the equivalent K_{mat} value was computed using the Wallin upper shelf correlation. For observed % shear values indicative of the transition region, the equivalent K_{mat} value was computed using the Master Curve method in API 579 Annex 9F.

https://doi.org/10.52202/072781-0005

Full-Scale Testing

All samples listed in **Table 1** were subjected to full-scale testing to record the burst pressure and determine if fatigue cracks initiated and propagated during the testing. Fatigue testing consisted of pressurizing each sample to produce a cyclic hoop stress of ~36% SMYS (100 psig to 100 psig + 36% SMYS) for 25,000 cycles or until a leak or rupture was observed. All samples that did not exhibit a failure during fatigue testing were then pressurised until failure.

Table 6 contains a summary of the full-scale testing results. Of the 16 samples subjected to fatigue testing, one leak was observed for sample AO2 after the completion of 17,749 cycles, as shown in **Figure 2**. No leaks or ruptures were observed for any of the other 15 samples.

Table 6. Full-Scale Testing Results Summary

Sample No.	Seam Type	Outside Diameter (OD), inch	Wall Thickness (WT), inch	Feature Depth, %WT	Feature Width	Cycles Completed	Observed Burst Pressure, psig
LF1	LF ERW	10.75	0.219	30 %	1 x WT	19,257[1]	3,548
LF2				50 %	1 x WT	25,000	2,918
LF3				30 %	3 x WT	25,000	3,446
LF4				50 %	3 x WT	25,000	2,986
HF1	HF ERW	12.75	0.250	30 %	1 x WT	25,000	2,898
HF2				50 %	1 x WT	25,000	2,418
HF3				30 %	3 x WT	25,000	2,688
HF4				50 %	3 x WT	25,000	2,321
AO1	EFW (AO Smith)	12.75	0.250	30 %	1 x WT	25,000	2,038
AO2				50 %	1 x WT	17,749[2]	N/A
AO3				30 %	3 x WT	25,000	2,574
AO4				50 %	3 x WT	25,000	1,927
DSAW1	DSAW	18.0	0.312	30 %	1 x WT	25,000	2,817
DSAW2				50 %	1 x WT	25,000	2,437
DSAW3				30 %	3 x WT	25,000	2,568
DSAW4				50 %	3 x WT	25,000	2,524

[1] A cycle count error resulted in only 19,257 cycles being run.
[2] A leak was observed after 17,749 cycles.

https://doi.org/10.52202/072781-0005

Figure 2. Leak observed in sample AO2 after 17,749 cycles.

Post-Test Fractography

Post-test fractography indicated that all samples (with the exception of sample AO2, which leaked during fatigue testing) exhibited ductile failure during the burst test. Distinct chevrons pointing back to the notch were observed, and the large amount of plastic deformation and fish-mouth fractures were consistent with ductile overload. No seam flaws were identified along any of the fracture surfaces.

Two of the 16 samples showed evidence of fatigue propagation: AO2 (which leaked during the fatigue testing) and DSAW2. Note, these samples contained the deepest and narrowest corrosion features, thereby introducing the highest potential for geometry-induced constraint.

For sample AO2, ratchet marks were observed along the boundary between the notch and fracture, and propagation was observed through the remaining WT beneath the EDM notch, as shown in **Figure 3**. For sample DSAW2, ratchet marks were observed along the boundary between the notch and fracture, and propagation was observed for a depth up to 0.022 inch beneath the EDM notch, as shown in **Figure 4**.

https://doi.org/10.52202/072781-0005

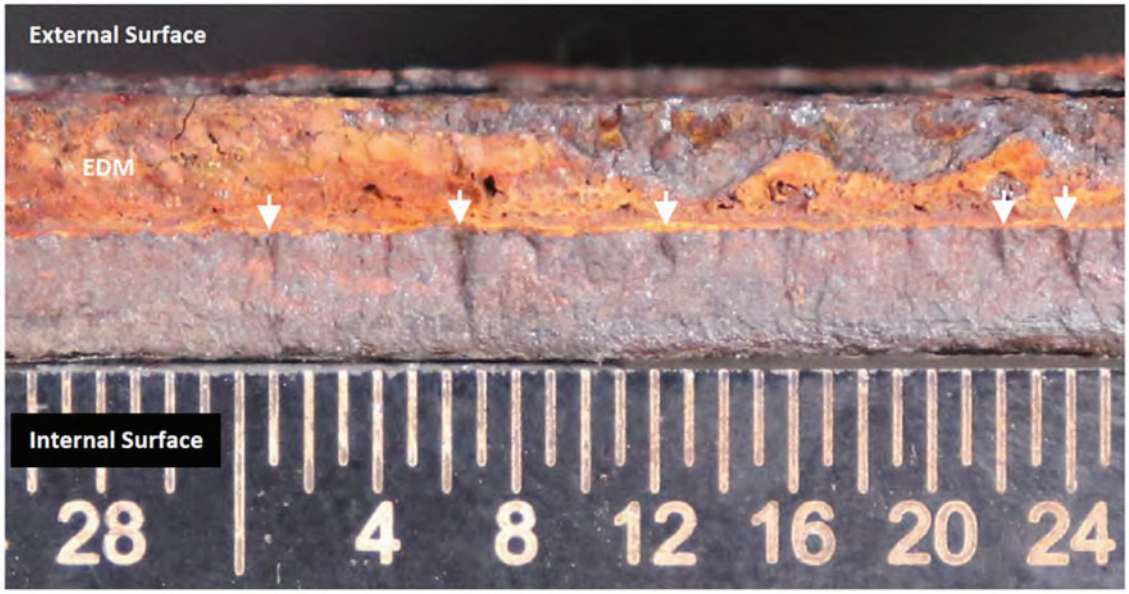

Figure 3. Fracture surface, sample AO2.

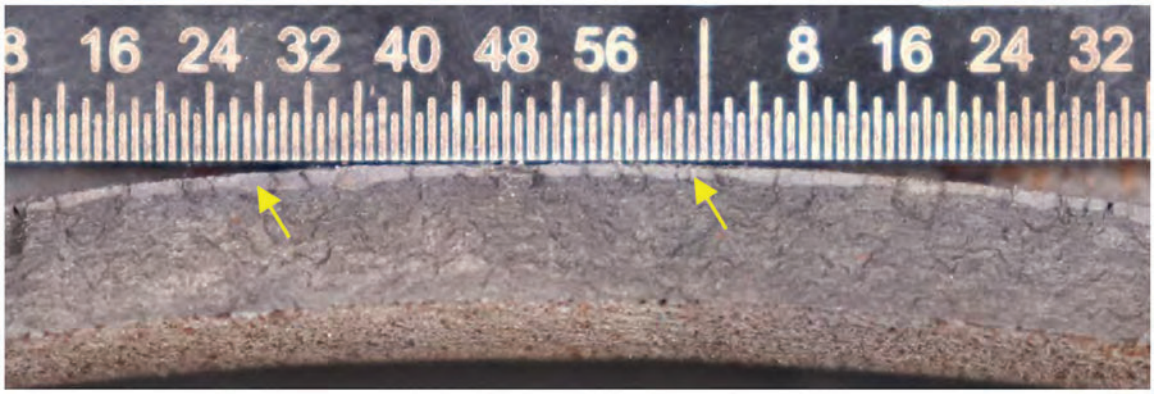

Figure 4. Fracture surface, sample DSAW2.

Detailed Engineering Analysis

ASME B31G Burst Pressure Calculations

Following the completion of the full-scale testing, the critical thickness profiles extracted from the Creaform laser scan data were used to execute burst pressure calculations for each sample based on the methodology contained in ASME B31G [16]. **Table 7** summarizes these results.

For all samples subjected to burst testing, the observed burst pressures were consistent with, or significantly exceeded, what would be predicted from ASME B31G. Sample AO1 was the only sample for which some of the computed burst pressures were slightly lower than the observed burst pressure.

https://doi.org/10.52202/072781-0005

In this instance, the maximum difference between the computed burst pressure and observed burst pressure was 6.5% (2,170 psig computed versus 2,038 psig observed).

Table 7. ASME B31G Burst Pressure Results Summary

Sample No.	Seam Type	Feature Depth, %WT	Feature Width	Observed Burst Pressure, psig	Computed Burst Pressure[1], psig	
					Considering SMYS	Considering Actual Measured SMYS
LF1	LF ERW	30 %	1 x WT	3,548	2,095 to 2,125	2,487 to 2,522
LF2		50 %	1 x WT	2,918	1,851 to 1,910	2,197 to 2,267
LF3		30 %	3 x WT	3,446	2,083 to 2,137	2,472 to 2,536
LF4		50 %	3 x WT	2,986	1,761 to 1,864	2,090 to 2,212
HF1	HF ERW	30 %	1 x WT	2,898	2,156 to 2,173	2,608 to 2,628
HF2		50 %	1 x WT	2,418	1,844 to 1,845	2,231 to 2,232
HF3		30 %	3 x WT	2,688	1,988 to 2,039	2,405 to 2,467
HF4		50 %	3 x WT	2,321	1,649 to 1,761	1,995 to 2,131
AO1	EFW (AO Smith)	30 %	1 x WT	2,038	2,092 to 2,125	2,136 to 2,170
AO2		50 %	1 x WT	N/A	1,867 to 1,887	1,906 to 1,927
AO3		30 %	3 x WT	2,574	2,028 to 2,062	2,070 to 2,106
AO4		50 %	3 x WT	1,927	1,749 to 1,753	1,785 to 1,789
DSAW1	DSAW	30 %	1 x WT	2,817	1,882 to 1,887	2,234 to 2,240
DSAW2		50 %	1 x WT	2,437	1,762 to 1,809	2,092 to 2,148
DSAW3		30 %	3 x WT	2,568	1,924 to 1,937	2,284 to 2,299
DSAW4		50 %	3 x WT	2,524	1,693 to 1,711	2,010 to 2,031

[1] Burst pressures were computed considering the detailed laser scan data using ASME B31G modified and effective area.

Finite Element Analysis – Calibration Phase

To ensure that the observations from the full-scale testing could be expected for other potential combinations of pipe dimensions and grade, elastic-plastic FEA was conducted based on the Creaform laser scan data and the material property testing results collected prior to the full-scale testing. As an initial calibration step, FEA models were developed for each of the 16 corrosion features to confirm consistency between the FEA results and the observed burst pressures.

Two potential failure mechanisms were evaluated to predict failure based on the FEA results: plastic collapse and local failure. Plastic collapse was evaluated by analysing the relationship between the applied internal pressure load and resulting radial displacement of the pipe subjected to the internal pressure load. Plastic collapse is predicted when a small increase in internal pressure results in a very large increase in radial displacement, ultimately leading to the FEA no longer being able to converge on a solution.

https://doi.org/10.52202/072781-0005

Local failure was evaluated based on the guidelines contained in API 579 Annex 2D.3.3 and ASME BPVC VIII-2 Section 5.3.3 [17]. This consists of computing an allowable plastic strain as a function of the mean stress and stress triaxiality at a given location. This allowable plastic strain is computed at all nodes contained within the FEA model and then compared to the computed equivalent plastic strain at that same node. Failure is predicted when the equivalent plastic strain exceeds the allowable plastic strain. To evaluate local failure, a parameter referred to as DUCTCRT was defined as the ratio of the equivalent plastic strain and the allowable plastic strain. Therefore, local failure is predicted to occur when DUCTCRT ≥ 1.0.

Figure 5 exemplifies how plastic collapse and local failure were evaluated for sample AO1. For this sample, the DUCTCRT reached 1.0 prior to exhibiting plastic collapse behavior, indicating that local failure was the controlling failure mechanism. Local failure was predicted to occur (i.e., DUCTCRT = 1.0) at 2,137 psig. This predicted failure pressure exceeded the actual observed pressure (2,038 psig) by less than 5%, indicating the FEA model provided a reasonably consistent prediction compared to the actual observed results. **Figure 6** and **Figure 7** provide screenshots of the computed von Mises stress and equivalent plastic strain at a pressure approaching the predicted local failure pressure.

Plastic collapse and local failure were evaluated in a similar manner for the other 14 samples subjected to burst testing (recall sample AO2 leaked during fatigue testing and was, therefore, not subjected to burst testing). **Table 8** provides a summary of the failure pressures predicted from FEA compared to the observed failure pressures.

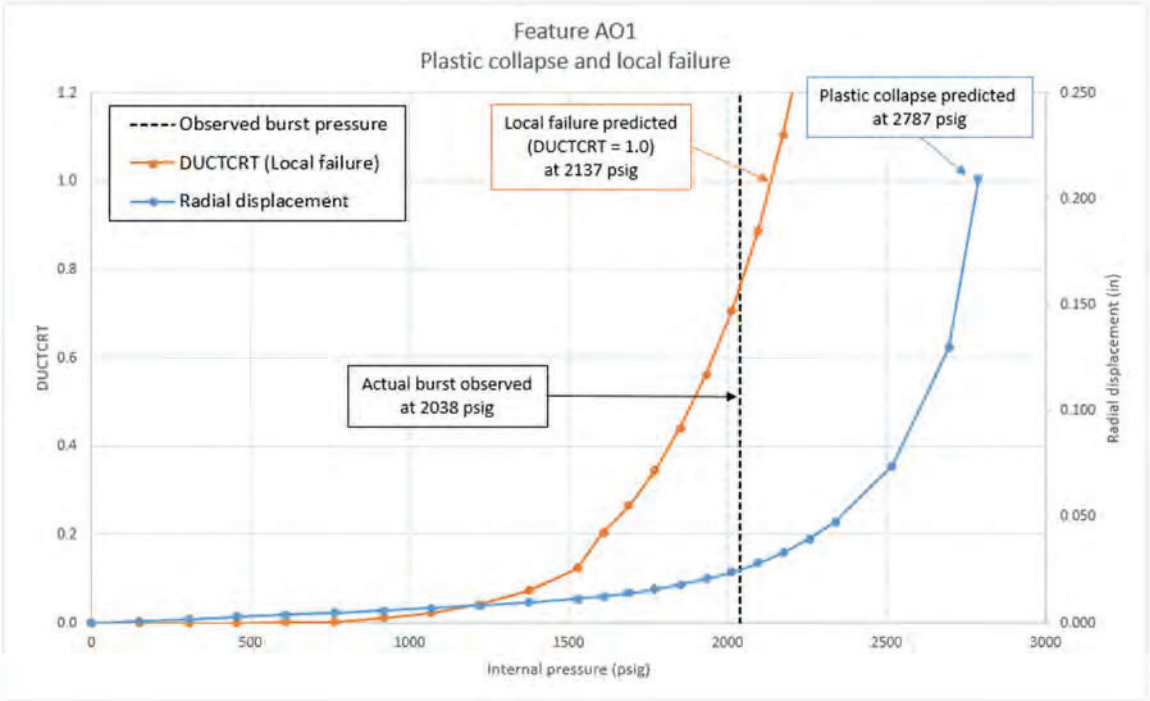

Figure 5. Evaluation of plastic collapse and local failure, sample AO1

https://doi.org/10.52202/072781-0005

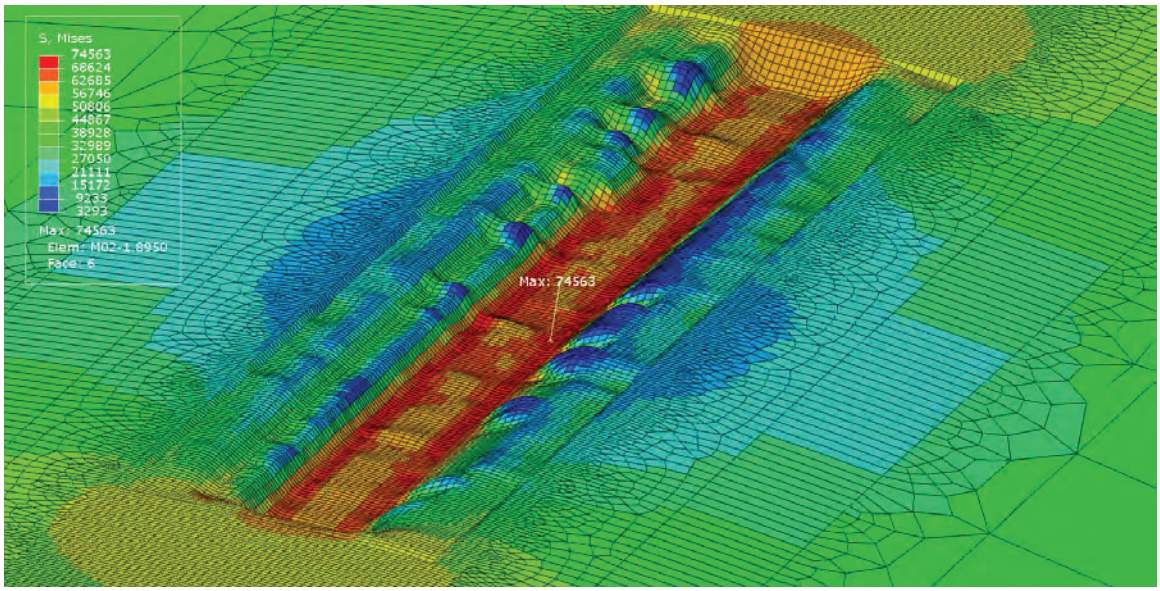

Figure 6. Von Mises stress (psi) at pressure approaching the predicted local failure pressure, sample AO1.

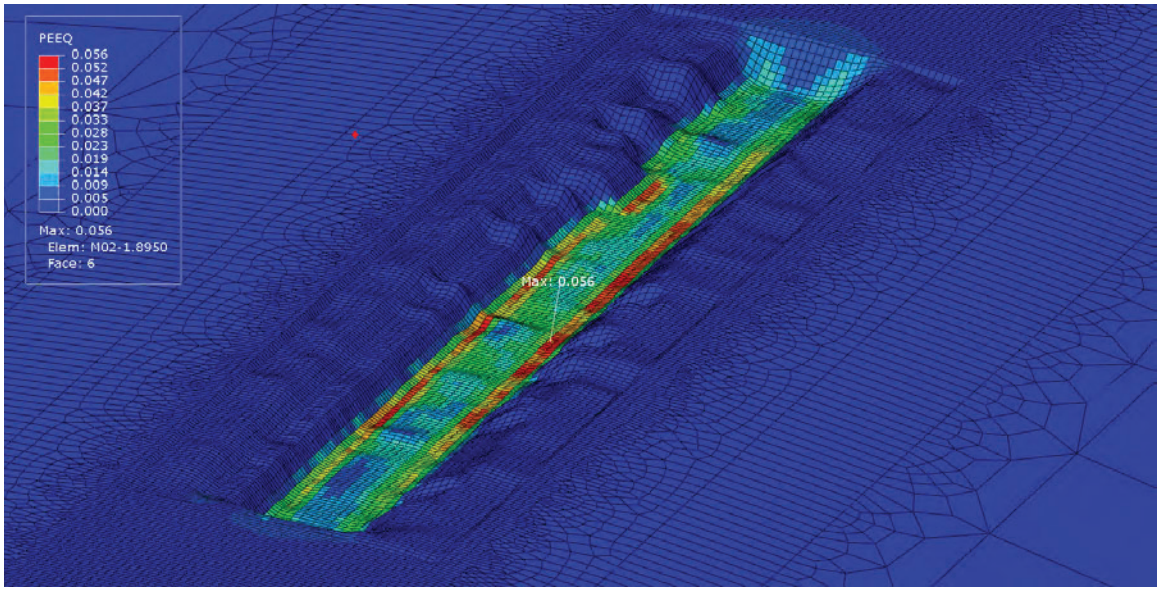

Figure 7. Equivalent plastic strain (inch/inch) at pressure approaching the predicted local failure pressure, sample AO1.

https://doi.org/10.52202/072781-0005

Table 8. Comparison of failure pressures predicted from FEA and actual observed failure pressures.

Sample No.	Seam Type	Feature Depth, %WT	Feature Width	Observed Failure Pressure, psig	Predicted Failure Pressure, psig	% Error[1]
LF1	LF ERW	30 %	1 x WT	3,548	3,378 (plastic collapse)	4.8 %
LF2		50 %	1 x WT	2,918	2,982 (plastic collapse)	-2.2 %
LF3		30 %	3 x WT	3,446	3,361 (plastic collapse)	2.5 %
LF4		50 %	3 x WT	2,986	3,026 (plastic collapse)	-1.3 %
HF1	HF ERW	30 %	1 x WT	2,898	2,642 (local failure)	8.8 %
HF2		50 %	1 x WT	2,418	2,626 (plastic collapse)	-8.6 %
HF3		30 %	3 x WT	2,688	2,514 (local failure)	6.5 %
HF4		50 %	3 x WT	2,321	2,493 (plastic collapse)	-7.4 %
AO1	EFW (AO Smith)	30 %	1 x WT	2,038	2,137 (local failure)	-4.8 %
AO2		50 %	1 x WT	N/A	N/A	N/A
AO3		30 %	3 x WT	2,574	2,247 (local failure)	12.7 %
AO4		50 %	3 x WT	1,927	1,898 (local failure)	1.5 %
DSAW1	DSAW	30 %	1 x WT	2,817	2,727 (plastic collapse)	3.2 %
DSAW2		50 %	1 x WT	2,437	2,519 (plastic collapse)	-3.4 %
DSAW3		30 %	3 x WT	2,568	2,554 (plastic collapse)	0.5 %
DSAW4		50 %	3 x WT	2,524	2,517 (plastic collapse)	0.3 %

[1] A positive % error indicates the FEA under-predicted the failure pressure compared to the actual observed results, while a negative % error indicates the FEA over-predicted the failure pressure.

The results presented in Table 8 show strong agreement between the failure pressures predicted from FEA and the observed failure pressures. All computed failure pressures exhibited less than 10% with the exception of sample AO3, which conservatively under-predicted the failure pressure by 12.7%. The largest over-prediction of burst pressure was 8.6%, corresponding to sample HF2.

The results from the calibration phase provided confidence that the methods used to compute failure pressure produce a reliable prediction when compared to observed results. Furthermore, the FEA results were consistent with the observation from previous phases of this project that the application of a traditional metal loss model such as ASME B31G provided a reasonable (and often conservative) estimate of remaining strength of these features.

Finite Element Analysis – Prediction Phase

The methodology discussed in the previous section was utilized to predict the failure pressure for an additional 15 samples. For these new models, the same laser scan data were utilized to generate an FEA mesh. However, these new analyses considered pipe dimensions with larger diameter to thickness (D/t) ratios and lower grades. The objective of this additional analysis was to confirm whether the behavior observed from previous phases of this project would be expected for other potentially more critical combinations of pipe size and grade. **Table 9** summarizes the additional analysis cases considered.

https://doi.org/10.52202/072781-0005

Table 9. Additional analysis cases considered.

Model No.	Seam Type	OD, inch	WT, inch	D/t	YS, psi	UTS, psi	Feature Depth[1], %WT	Feature Width
LF1-1	LF ERW	16.0	0.188	85.1	35,000	60,000	30 %	1 x WT
LF2-1							50 %	1 x WT
LF3-1							30 %	3 x WT
LF4-1							50 %	3 x WT
HF1-1	HF ERW	24.0	0.250	96.0	35,000	60,000	30 %	1 x WT
HF2-1							50 %	1 x WT
HF3-1							30 %	3 x WT
HF4-1							50 %	3 x WT
AO1-1	EFW (AO Smith)	36.0	0.312	115.4	35,000	60,000	30 %	1 x WT
AO3-1							30 %	3 x WT
AO4-1							50 %	3 x WT
DSAW1-1	DSAW	42.0	0.375	112.0	35,000	60,000	30 %	1 x WT
DSAW2-1							50 %	1 x WT
DSAW3-1							30 %	3 x WT
DSAW4-1							50 %	3 x WT

[1] The laser scan data were scaled such that the individual depth percentage values as a function of the wall thickness remained the same as the original data set.

Table 10 summarizes the FEA-predicted burst pressures and the corresponding burst pressures computed per ASME B31G modified and effective area. The results indicated that for all 15 cases, the ASME B31G modified and effective area methods provided a conservative estimate of burst pressure compared to FEA. Given the strong agreement between the failure pressures predicted from FEA and the actual observed failure pressures from the full-scale testing, it can be concluded that the ASME B31G modified and effective area methods would be expected to provide a conservative estimate of each theoretical feature's true burst pressure.

https://doi.org/10.52202/072781-0005

Table 10. Comparison of FEA-predicted burst pressures and burst pressures computed per ASME B31G modified and effective area.

Model No.	Feature Depth, %WT	Feature Width	Computed Burst Pressure, psig		
			FEA	ASME B31G Modified	Effective Area
LF1-1	30 %	1 x WT	1,069	898	904
LF2-1	50 %	1 x WT	830	822	796
LF3-1	30 %	3 x WT	1,143	910	888
LF4-1	50 %	3 x WT	993	799	758
HF1-1	30 %	1 x WT	1,057	858	864
HF2-1	50 %	1 x WT	871	763	762
HF3-1	30 %	3 x WT	999	824	808
HF4-1	50 %	3 x WT	899	742	702
AO1-1	30 %	1 x WT	861	729	724
AO3-1	30 %	3 x WT	877	712	712
AO4-1	50 %	3 x WT	786	662	661
DSAW1-1	30 %	1 x WT	879	765	766
DSAW2-1	50 %	1 x WT	860	735	726
DSAW3-1	30 %	3 x WT	915	761	763
DSAW4-1	50 %	3 x WT	808	713	710

Summary and Conclusions

The research and analysis presented herein, along with additional relevant past research, supports that if no preferential attack of the bondline is occurring, the remaining strength of a corrosion anomaly on product lines is not affected by the presence of an LSW, even in the presence of significant fatigue cycling. Furthermore, the application of traditional metal loss assessment methodologies such as ASME B31G modified and effective area are expected to provide a reliable estimate of burst pressure. This statement is based on careful consideration of the following factors:

- Ductility of the seam weld:
    - For a traditional metal loss model to be appropriate, the feature must be expected to fail due to plastic collapse. However, this may not be an appropriate assumption for seam welds with very low toughness.
    - The analysis and research presented herein identified that seam welds containing metal loss with a 0.33-subsize CVN impact energy as low as 1.5 ft-lbs, or a fracture toughness as low as 35,307 psi√inch could demonstrate plastic collapse.

- Constraint effects from the feature geometry:
    - In general, higher constraint is expected in narrow, deep features as opposed to wide, shallow features.

https://doi.org/10.52202/072781-0005

  - When the material behavior is expected to be ductile, ASME B31G applies to all seam weld metal loss (excluding SSWC) without considering any constraint effect
  - Even when material toughness is low (e.g., some pre-1967 seam welds), the analysis and research presented herein identified that constraint effects are not likely to be a concern for features with a width greater than or equal to the wall thickness, given the depth is 30% or less. Furthermore, for features with a width greater than or equal to 3 times the wall thickness, features with a depth of 50% or less are not likely to experience any issues related to constraint.

- Existence of pre-existing manufacturing defects at the location of the corrosion:
  - The presence of pre-existing manufacturing defects (such as hook cracks, lack of fusion, cold welds, etc.) have the potential to support crack development within a metal loss feature in the context of significant fatigue cycling, which can, in turn, lead to non-conservative prediction of burst pressure when using traditional metal loss models.

These conclusions are based on experiments in which very aggressive pressure cycling was simulated and, therefore, could be conservative when applied to pipelines exhibiting less aggressive cyclic operation. In addition to the factors discussed above, understanding a pipeline's susceptibility to SSWC and the ability to reliably differentiate corrosion preferential to, versus coincident with, a longitudinal seam is an important topic and the subject of ongoing research. The following sibling projects are continuing these research efforts: EC-02-12 "Evaluation of Selective Seam Weld Corrosion Susceptibility," NDE-4-13 "Selective Seam Weld Corrosion Detection with In-line Inspection Technologies," IM-3-03 "Comprehensive Review and Assessment Guidelines for SSWC," IM-1-08 "Pragmatic Application of MegaRule RIN 1 - 192.712 Toughness Values," and NDE-2-15 "SSWC Identification, Sizing, and Measuring Grooving Ratio In the Ditch."

References

[1] B. Leis and X.-K. Zhu, "Corrosion Assessment Criteria: Rationalizing Their Use for Vintage vs. Modern Pipelines," US DOT Research and Special Projects Agency, Contract No. TRSS56-03-T-0014, September 2005.

[2] B. N. Leis, E. B. Clark, X. K. Zhu and R. D. Galliner, "Guidelines for Assessing Corrosion Associated with Girth and Long-Seam Welds," PRCI Report GRI-8521, 2004.

[3] B. N. Leis, E. B. Clark, X. K. Zhu and R. D. Galliner, "IPC2006-10503 Guidelines for Assessing Corrosion Associated with Welds," in International Pipeline Conference, 2006.

[4] J. F. Keifner and K. M. Kolovich, "ERW and Flash Weld Seam Failures," Subtask 1.4 Department of Transportation Agreement No. DTPH56-11-0003, 2012.

https://doi.org/10.52202/072781-0005

[5] B. N. Leis and J. B. Nestleroth, "Batelle's Experience with ERW ad Flash Weld Seam Failures: Causes and Implications," Subtask 1.4 US Department of Transportation Agreement No. DTPH56-11-0003, 2012.
[6] J. F. Keifner and et al, "Review of ERW Pipe Burst Test Data," Subtask 2.2 US Department of Transportation Agreement No. DTPH56-11-0003, 2013.
[7] J. F. Keifner, "Modified Equation Helps Integrity Management," Oil and Gas Journal, 06 October 2008.
[8] J. F. Keifner, "Fracture Initiation," in 4th Symposium on Line Pipe Research, American Gass Association, Catalog No. L30075, 1969.
[9] G. M. Wilkowski and et al, "PR276-04502, Failure Initiation Modes of Pipe with High Charpy Transition Temperature," Pipeline Research Council International, 2007.
[10] P. A. Zelenak and J. F. Keifner, "IPC04-0129, Test Behavior of Low-Toughness Pipe Affected by Corrosion Defects," in International Pipeline Conference, Calgary, AB, 2004.
[11] M. J. Rosenfeld, "Accepting Metal Loss Corrosion on Longitudinal Seams," in Pipeline Pigging and Integrity Management Conference, Houston, TX, Feb. 2-4, 2022.
[12] American Society of Mechanical Engineers, API 579-1/ASME FFS-1 Fitness-for-Service, Washington, D.C.: API Publishing Services, 2021.
[13] G. W. Brown, T. L. Anderson, L. Parietti and B. Rose, "Evaluation of Groove Radius Assessment Criteria Based one Brittle and Ductile Local Failure Modes," in ASME Pressure Vessels and Piping Conference, Vancouver, British Columbia, Canada, 2016.
[14] American Petroleum Institute, API 1163: In-line Inspection Systems Qualification, Washington, DC: API Publishing Services, 2018.
[15] American Society for Testing and Materials, ASTM E1820 Standard Test Method for Measurement of Fracture Toughness, West Conshohocken, PA: ASTM International.
[16] American Society of Mechanical Engineers, ASME B31.G Manual for Determining the Remaining Strength of Corroded Pipelines, West Conshohocken, PA: ASME International, 2012.
[17] American Society of Mechanical Engineers, ASME BPVC Section VIII Division 2, New York: ASME International, 2021.

https://doi.org/10.52202/072781-0005